Multi-Satellite Time-Delay Estimation for Reliable High-Resolution GNSS Receivers

Christoph Enneking*, Manuel Stein†, Mario Castañeda†, Felix Antreich‡, Josef A. Nossek†
†Institute for Circuit Theory and Signal Processing, *Technische Universität München, Munich, Germany
‡Institute for Communications and Navigation, Deutsches Zentrum für Luft- und Raumfahrt, Weßling, Germany
Email: {Stein, Nossek}@nws.ei.tum.de

***Abstract*—Reliable estimation of position in time and space has become a key necessity in several technical applications like mobile navigation, precision farming or network synchronization. While the increasing amount of operating Global Navigation Satellite Systems (GNSS) offers diverse possibilities to receive GNSS signals worldwide and to determine position accurately, inter- and intrasystem interference has been identified as a problem of growing importance. The performance of receivers which track all in-view satellites individually degrades if mutual interference is not taken into account. Therefore, we consider the problem of joint signal parameter estimation. For scenarios where the signals of different satellites superimpose at the receiver a joint maximum likelihood estimator for all relevant signal parameters is derived. In order to keep the computation of the related likelihood function, and the determination of its maximum, feasible for a low-complexity receiver, an iterative Expectation-Maximization (EM) algorithm is applied. Simulations for different scenarios show that this approach is efficient in the estimation theoretic sense, and robust against interference that is caused by signals with known structure.**

***Index Terms*—global positioning system, channel estimation, multiple access interference**

I. Introduction

INTERFERENCE is more and more becoming a problem in Global Navigation Satellite Systems (GNSS). Different systems like GPS or the forthcoming Galileo and Compass occupy the same radio frequency (RF) bands, whether for the sake of interoperability or due to shortage on available carrier frequencies. As a consequence, the relevant RF bands are occupied by an increasing number of satellites of different systems causing *intersystem* interference (Fig. 1) for GNSS receivers. Besides intersystem interference, the satellite signals of a single system interfere with each other when centered around the same carrier frequency. This *intrasystem* interference (Fig. 1) is considerable since the number of in-view satellites of a single fully operational GNSS can be as large as twelve or higher.

Both kinds of interference have in common that they result from the joint transmission of multiple transmitters at the same time on the same frequency band. The signals of K distinct line-of-sight (LOS) satellites superimpose at the receive antenna. While the receiver aims to specify the signal parameters like time-of-arrival (TOA) and carrier-phase of each signal component, the estimation of these parameters is disturbed by thermal noise of the analog radio components. Additionally, the signal components affect the parameter estimation accuracy among each other due to multiple access interference (MAI). A similar problem arises in wireless CDMA communication systems [1] [2].

The compatibility of different satellites and systems is achieved today by spread-spectrum and pulse-shaping methods. Pseudo-random (PR) spreading sequences with low cross-correlation are assigned to each satellite in attempt to orthogonalize multiple access and through different versions of binary-offset carrier (BOC) modulation signal power is split in the frequency domain. While synchronization of the transmitting satellites is possible, the satellite signals arrive asynchronously at different receivers. The dependence of individual signal parameters like time and Doppler-shift on the receivers position and their relative velocities makes it impossible to ensure full separation of satellite signals for all users.

A possible solution to combat intersystem interference could be to increase the signal power of a certain system. While this might lead to an improved performance of the associated receivers, the performance of other systems will degrade due to a higher interference level. As an alternative, political debates could lead to a partitioning of the available frequency bands that would allow to operate different systems under tolerable intersystem interference.

However, we propose a technical solution to the problem of inter- and intrasystem interference which is based solely on the receiver. Instead of performing range measurements for each satellite separately this task is formulated as a joint channel parameter estimation problem. An iterative algorithm ensures computational complexity of the presented approach that is comparable to a separate approach forming the basis of today's GNSS receivers. Simulations show that when all signals are tracked jointly inter- and intrasystem interference can be widely suppressed. This result suggests, that if coarse signal acquisition is guaranteed, one can optimize the satellite signals with respect to parameter estimation performance [3] [4] without trading off their effect onto other systems or signals. The only requirement is that the structure of all transmit signals has to be available at the receiver.

II. Outline

The paper is organized as follows. First we summarize related works and introduce the notation. Then, a system model with K superimposed LOS satellite signals and a single receive antenna is defined. An estimation theoretical derivation yields an iterative joint parameter estimation procedure while

978-1-4673-0387-3/12/$31.00 ©2012 IEEE

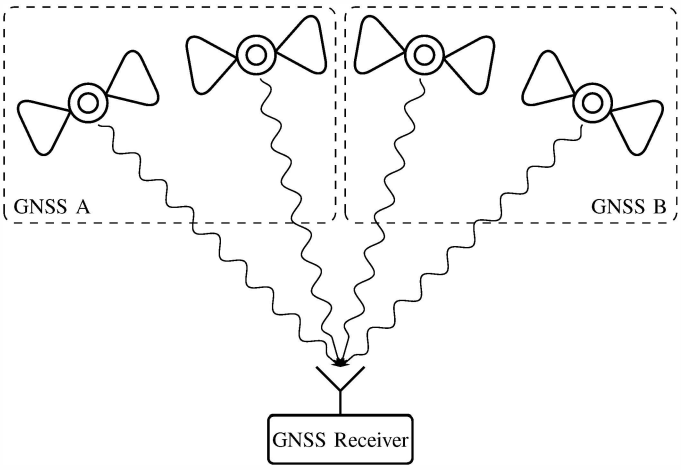

Fig. 1. GNSS inter- and intrasystem interference

the Cramér-Rao Lower Bound (CRLB) provides a theoretical performance benchmark. For completeness we review a separate estimation approach which is approximated by conventional GNSS receivers. For simulations we focus on GPS intrasystem and GPS - Galileo intersystem interference and compare the performance of the proposed and the conventional time-delay estimation (TDE) approaches for different GNSS scenarios.

III. Related Work

Solving a ML estimator [5] which is formulated directly for the position in three-dimensional space through the SAGE algorithm [6] is investigated in [7] where [8] tracks the signal parameters through a ML estimator on a linearized receive signal model. [9] summarizes the concept of Vector Tracking [10] and Joint Tracking loops and introduces the idea of Position Domain Joint Tracking loops in order to track the carrier-phases and estimate the receivers location in parallel while [11] compares Vector Tracking loops to Scalar Tracking loops. The potential of ML-based parameter estimation with a multi-antenna receiver in the presence of multi-path propagation is shown in [12] [13] [14] [15]. [16] discusses the challenges of using GNSS in indoor scenarios and reviews the foundations of GNSS signal processing. [17] sheeds light on the typical intersystem interference levels through an analytical model provided by the International Telecommunication Union (ITU).

IV. Notation

Throughout this work scalars are defined as lower case letters, whereas column vectors and matrices are defined with lower case bold letters and upper case bold leters, respectively. In addition, $\arg(x)$ denotes the phase of the scalar x. The real and imaginary part of a scalar x are defined by $\mathrm{Re}\{x\}$ and $\mathrm{Im}\{x\}$. $\boldsymbol{A}\odot\boldsymbol{B}$ represents the Hadamar-Schur product or entry-wise product, while $\|\boldsymbol{x}\|$ denotes the Euclidean norm of $\boldsymbol{x}$. The Moore-Penrose pseudoinverse of the matrix $\boldsymbol{A}$ is given as $\boldsymbol{A}^{+}$ while $\mathrm{diag}(\boldsymbol{a})$ yields a matrix with the elements of $\boldsymbol{a}$ on its diagonal.

V. System Model

The analog GNSS receive signal in baseband representation

$$y(t) = \sum_{k=1}^{K} s_k(t, \boldsymbol{\theta}_k) + n(t) \tag{1}$$

consists of K satellite signals and additive Gaussian noise $n(t)$. The signal components $s_k(t)$ have the form

$$s_k(t, \boldsymbol{\theta}_k) = \gamma_k \, \mathrm{e}^{\mathrm{j}2\pi\nu_k t} \, c_k(t - \tau_k) \tag{2}$$

where $c_k(t) \in \mathbb{C}$ denotes the transmit signal of the k-th satellite and is assumed to be available at the receiver. Each satellite signal arrives at the receiver with unkown time-delay τ_k, unknown Doppler-frequency shift ν_k, unknown attenuation $|\gamma_k|$ and carrier-phase $\arg(\gamma_k)$. The parameters of the k-th satellite signal are summarized by

$$\boldsymbol{\theta}_k = [\tau_k, \nu_k, \mathrm{Re}\{\gamma_k\}, \mathrm{Im}\{\gamma_k\}]^T \in \mathbb{R}^4. \tag{3}$$

Sampling the received signal with $T_s = 1/2B$ after an ideal low-pass filter with one-sided bandwidth B yields N observations

$$\boldsymbol{y} = \sum_{k=1}^{K} \boldsymbol{s}_k(\boldsymbol{\theta}_k) + \boldsymbol{n}, \tag{4}$$

where

$$\begin{aligned} \boldsymbol{y} &= [y(0), y(T_s), \ldots, y((N-1)T_s)]^T \in \mathbb{C}^N \\ \boldsymbol{s}_k(\boldsymbol{\theta}_k) &= [s_k(0, \boldsymbol{\theta}_k), s_k(T_s, \boldsymbol{\theta}_k), \ldots, s_k((N-1)T_s, \boldsymbol{\theta}_k)]^T \in \mathbb{C}^N \\ \boldsymbol{n} &= [n(0), n(T_s), \ldots, n((N-1)T_s)]^T \in \mathbb{C}^N. \end{aligned} \tag{5}$$

Defining the vectors

$$\begin{aligned} \boldsymbol{\tau} &= [\tau_1, \tau_2, \ldots, \tau_K]^T \in \mathbb{R}^K \\ \boldsymbol{\nu} &= [\nu_1, \nu_2, \ldots, \nu_K]^T \in \mathbb{R}^K \\ \boldsymbol{\gamma} &= [\gamma_1, \gamma_2, \ldots, \gamma_K]^T \in \mathbb{C}^K, \end{aligned} \tag{6}$$

the sum of all LOS signals can be expressed by

$$\sum_{k=1}^{K} \boldsymbol{s}_k(\boldsymbol{\theta}_k) = (\boldsymbol{C}(\boldsymbol{\tau}) \odot \boldsymbol{D}(\boldsymbol{\nu}))\boldsymbol{\gamma}, \tag{7}$$

where

$$\begin{aligned} \boldsymbol{C}(\boldsymbol{\tau}) &= [\boldsymbol{c}_1(\tau_1), \boldsymbol{c}_2(\tau_2), \ldots, \boldsymbol{c}_K(\tau_K)] \\ \boldsymbol{c}_k(\tau_k) &= [c_k(-\tau_k), c_k(T_s - \tau_k), \ldots, c_k((N-1)T_s - \tau_k)]^T \end{aligned} \tag{8}$$

contains the sampled and shifted versions of the satellite signals $c_k(t)$ and $\boldsymbol{D}(\boldsymbol{\nu}) \in \mathbb{C}^{N\times K}$ encapsulates the Doppler frequencies for all impinging signal components

$$\begin{aligned} \boldsymbol{D}(\boldsymbol{\nu}) &= [\boldsymbol{d}(\nu_1), \boldsymbol{d}(\nu_2), \ldots, \boldsymbol{d}(\nu_K)] \\ \boldsymbol{d}(\nu_k) &= \left[1, e^{\mathrm{j}2\pi\nu_k T_s}, \ldots, e^{\mathrm{j}2\pi\nu_k (N-1)T_s}\right]^T. \end{aligned} \tag{9}$$

As the additive noise $n(t)$ is assumed to be zero-mean, unit variance, complex circularly-symmetric Gaussian and temporally white and the ideally lowpass filtered receive signal is

sampled at Nyquist rate, the noise samples $\boldsymbol{n}$ satisfy

$$\begin{aligned} \mathrm{E}\left[\boldsymbol{n}\right] &= \boldsymbol{0} \\ \mathrm{E}\left[\boldsymbol{n}\boldsymbol{n}^H\right] &= \boldsymbol{I} \\ \mathrm{E}\left[\boldsymbol{n}\boldsymbol{n}^T\right] &= \boldsymbol{0}. \end{aligned} \tag{10}$$

Therefore, the parameterized probability density function (pdf) of the received signal $\boldsymbol{y}$ is given by

$$\mathrm{p}(\boldsymbol{y};\boldsymbol{\theta}) = \frac{1}{\pi^N} \exp\left(- \left\| \boldsymbol{y} - \sum_{k=1}^{K} \boldsymbol{s}_k(\boldsymbol{\theta}_k) \right\|^2 \right). \tag{11}$$

VI. Parameter Estimation

In order to determine position in time and space, the receiver has to estimate its distance to each satellite through range measurements. This is achieved by determining the time-of-arrival (TOA) τ_k for each of the K signal components while the carrier-phase $\arg(\gamma_k)$ can be used for refining the estimation.

A. Maximum Likelihood (ML) Estimation

For the considered channel parameter estimation problem, the proposed procedure relies on formulating the estimator on the unknown parameter vector

$$\boldsymbol{\theta} = [\boldsymbol{\theta}_1^T \ \boldsymbol{\theta}_2^T \ \ldots \ \boldsymbol{\theta}_K^T]^T \in \mathbb{R}^{4K}. \tag{12}$$

With the nonlinear least squares function $\Lambda(\boldsymbol{\theta};\boldsymbol{y})$ the ML estimator $\hat{\boldsymbol{\theta}}_{\mathrm{ML}}$ is given by

$$\begin{aligned} \hat{\boldsymbol{\theta}}_{\mathrm{ML}} &= \arg\max_{\boldsymbol{\theta}} \ \mathrm{p}(\boldsymbol{y};\boldsymbol{\theta}) \\ &= \arg\min_{\boldsymbol{\theta}} \ \left\| \boldsymbol{y} - \sum_{k=1}^{K} \boldsymbol{s}_k(\boldsymbol{\theta}_k) \right\|^2 \\ &\triangleq \arg\min_{\boldsymbol{\theta}} \ \Lambda(\boldsymbol{\theta};\boldsymbol{y}). \end{aligned} \tag{13}$$

The channel coefficients $\hat{\boldsymbol{\gamma}}_{\mathrm{ML}}$ are obtained by setting the partial Wirtinger derivative to zero

$$\frac{\partial \Lambda(\boldsymbol{\theta};\boldsymbol{y})}{\partial \boldsymbol{\gamma}^*} = \boldsymbol{0}, \tag{14}$$

using (7) and solving for $\boldsymbol{\gamma}$

$$\hat{\boldsymbol{\gamma}}_{\mathrm{ML}} = (\boldsymbol{C}(\boldsymbol{\tau}) \odot \boldsymbol{D}(\boldsymbol{\nu}))^{+} \boldsymbol{y}. \tag{15}$$

Substituting this result into (13), the ML estimator of time-delays and Doppler-shifts requires to maximize a function $\Phi(\boldsymbol{\tau},\boldsymbol{\nu};\boldsymbol{y})$ over a $2K$-dimensional space

$$\begin{aligned} &(\hat{\boldsymbol{\tau}}_{\mathrm{ML}}, \hat{\boldsymbol{\nu}}_{\mathrm{ML}}) \\ &= \arg\max_{(\boldsymbol{\tau},\boldsymbol{\nu})} \ \boldsymbol{y}^H (\boldsymbol{C}(\boldsymbol{\tau}) \odot \boldsymbol{D}(\boldsymbol{\nu}))(\boldsymbol{C}(\boldsymbol{\tau}) \odot \boldsymbol{D}(\boldsymbol{\nu}))^{+} \boldsymbol{y} \\ &\triangleq \arg\max_{(\boldsymbol{\tau},\boldsymbol{\nu})} \ \Phi(\boldsymbol{\tau},\boldsymbol{\nu};\boldsymbol{y}). \end{aligned} \tag{16}$$

B. Separate Estimation

A separate parameter estimator, which is approximated in current GNSS recievers, is obtained by

$$\hat{\boldsymbol{\theta}}_{\mathrm{SEP}} \quad = \quad \begin{bmatrix} \arg\min_{\boldsymbol{\theta}_1} \|\boldsymbol{y} - \boldsymbol{s}_1(\boldsymbol{\theta}_1)\|^2 \\ \arg\min_{\boldsymbol{\theta}_2} \|\boldsymbol{y} - \boldsymbol{s}_2(\boldsymbol{\theta}_2)\|^2 \\ \vdots \\ \arg\min_{\boldsymbol{\theta}_K} \|\boldsymbol{y} - \boldsymbol{s}_K(\boldsymbol{\theta}_K)\|^2 \end{bmatrix}. \tag{17}$$

The separate estimator is equivalent to the ML estimator if $K = 1$. For $K > 1$ the separate multi-satellite parameter estimation ignores MAI and treats K independent problems of the form

$$\begin{aligned} &(\hat{\tau}_{k,\mathrm{SEP}}, \hat{\nu}_{k,\mathrm{SEP}}) \\ &= \arg\max_{(\tau,\nu)} \ \boldsymbol{y}^H (\boldsymbol{c}_k(\tau) \odot \boldsymbol{d}(\nu))(\boldsymbol{c}_k(\tau) \odot \boldsymbol{d}(\nu))^{+} \boldsymbol{y} \\ &= \arg\max_{(\tau,\nu)} \ \frac{\left| \boldsymbol{y}^H (\boldsymbol{c}_k(\tau) \odot \boldsymbol{d}(\nu)) \right|^2}{\left\| \boldsymbol{c}_k(\tau) \odot \boldsymbol{d}(\nu) \right\|^2} \\ &= \arg\max_{(\tau,\nu)} \ \frac{\left| \boldsymbol{y}^H (\boldsymbol{c}_k(\tau) \odot \boldsymbol{d}(\nu)) \right|}{\left\| \boldsymbol{c}_k(\tau) \right\|} \\ &\triangleq \arg\max_{(\tau,\nu)} \ \phi_k(\tau,\nu;\boldsymbol{y}) \end{aligned} \tag{18}$$

and

$$\hat{\gamma}_{k,\mathrm{SEP}} = \frac{(\boldsymbol{c}_k(\hat{\tau}_{k,\mathrm{SEP}}) \odot \boldsymbol{d}(\hat{\nu}_{k,\mathrm{SEP}}))^H \boldsymbol{y}}{\left\| \boldsymbol{c}_k(\hat{\tau}_{k,\mathrm{SEP}}) \right\|^2} \tag{19}$$

for $k = 1, \ldots, K$.

C. Lower Bound on Estimation Variance

The diagonal entries of the inverse Fisher information matrix (FIM) $\boldsymbol{F}^{-1}(\boldsymbol{\theta})$ provide a lower bound on the achievable variance of any unbiased estimator [18]. The ij-th entry of the FIM is calculated

$$[\boldsymbol{F}(\boldsymbol{\theta})]_{ij} = -\,\mathrm{E}\left[\frac{\partial^2 \ln \mathrm{p}(\boldsymbol{y};\boldsymbol{\theta})}{\partial\theta_i \partial\theta_j} \right], \quad i,j = 1,\ldots,4K, \tag{20}$$

where the partial derivatives are evaluated at the true parameter value and the expectation is taken with respect to $\mathrm{p}(\boldsymbol{y};\boldsymbol{\theta})$. This bound is known as the Cramér-Rao Lower Bound (CRLB). Note that $\hat{\boldsymbol{\theta}}_{\mathrm{SEP}}$ is, in general, not unbiased and therefore its performance can not be bounded by the CRLB. Using (20), the FIM can be divided into 16 $\mathbb{R}^{K\times K}$ blockmatrices

$$\boldsymbol{F}(\boldsymbol{\theta}) = \begin{bmatrix} \boldsymbol{F}_{\mathrm{Re}\{\boldsymbol{\gamma}\}\,\mathrm{Re}\{\boldsymbol{\gamma}\}} & \boldsymbol{F}_{\mathrm{Re}\{\boldsymbol{\gamma}\}\,\mathrm{Im}\{\boldsymbol{\gamma}\}} & \boldsymbol{F}_{\mathrm{Re}\{\boldsymbol{\gamma}\}\boldsymbol{\tau}} & \boldsymbol{F}_{\mathrm{Re}\{\boldsymbol{\gamma}\}\boldsymbol{\nu}} \\ \boldsymbol{F}^T_{\mathrm{Re}\{\boldsymbol{\gamma}\}\,\mathrm{Im}\{\boldsymbol{\gamma}\}} & \boldsymbol{F}_{\mathrm{Im}\{\boldsymbol{\gamma}\}\,\mathrm{Im}\{\boldsymbol{\gamma}\}} & \boldsymbol{F}_{\mathrm{Im}\{\boldsymbol{\gamma}\}\boldsymbol{\tau}} & \boldsymbol{F}_{\mathrm{Im}\{\boldsymbol{\gamma}\}\boldsymbol{\nu}} \\ \boldsymbol{F}^T_{\mathrm{Re}\{\boldsymbol{\gamma}\}\boldsymbol{\tau}} & \boldsymbol{F}^T_{\mathrm{Im}\{\boldsymbol{\gamma}\}\boldsymbol{\tau}} & \boldsymbol{F}_{\boldsymbol{\tau}\boldsymbol{\tau}} & \boldsymbol{F}_{\boldsymbol{\tau}\boldsymbol{\nu}} \\ \boldsymbol{F}^T_{\mathrm{Re}\{\boldsymbol{\gamma}\}\boldsymbol{\nu}} & \boldsymbol{F}^T_{\mathrm{Im}\{\boldsymbol{\gamma}\}\boldsymbol{\nu}} & \boldsymbol{F}^T_{\boldsymbol{\tau}\boldsymbol{\nu}} & \boldsymbol{F}_{\boldsymbol{\nu}\boldsymbol{\nu}} \end{bmatrix}, \tag{21}$$

where

$$
\begin{aligned}
\boldsymbol{F}_{\mathrm{Re}\{\boldsymbol{\gamma}\}\,\mathrm{Re}\{\boldsymbol{\gamma}\}} &= 2(\boldsymbol{C}(\boldsymbol{\tau}) \odot \boldsymbol{D}(\boldsymbol{\nu}))^H (\boldsymbol{C}(\boldsymbol{\tau}) \odot \boldsymbol{D}(\boldsymbol{\nu})) \\
\boldsymbol{F}_{\mathrm{Im}\{\boldsymbol{\gamma}\}\,\mathrm{Im}\{\boldsymbol{\gamma}\}} &= 2(\boldsymbol{C}(\boldsymbol{\tau}) \odot \boldsymbol{D}(\boldsymbol{\nu}))^H (\boldsymbol{C}(\boldsymbol{\tau}) \odot \boldsymbol{D}(\boldsymbol{\nu})) \\
\boldsymbol{F}_{\boldsymbol{\tau}\boldsymbol{\tau}} &= 2\boldsymbol{\Upsilon}^H(\boldsymbol{\tau},\boldsymbol{\nu})\boldsymbol{\Upsilon}(\boldsymbol{\tau},\boldsymbol{\nu}) \\
\boldsymbol{F}_{\boldsymbol{\nu}\boldsymbol{\nu}} &= 2\boldsymbol{\Psi}^H(\boldsymbol{\tau},\boldsymbol{\nu})\boldsymbol{\Psi}(\boldsymbol{\tau},\boldsymbol{\nu}) \\
\boldsymbol{F}_{\mathrm{Re}\{\boldsymbol{\gamma}\}\,\mathrm{Im}\{\boldsymbol{\gamma}\}} &= \boldsymbol{0} \\
\boldsymbol{F}_{\mathrm{Re}\{\boldsymbol{\gamma}\}\boldsymbol{\tau}} &= 2\,\mathrm{Re}\{(\boldsymbol{C}(\boldsymbol{\tau}) \odot \boldsymbol{D}(\boldsymbol{\nu}))^H \boldsymbol{\Upsilon}(\boldsymbol{\tau},\boldsymbol{\nu})\} \\
\boldsymbol{F}_{\mathrm{Re}\{\boldsymbol{\gamma}\}\boldsymbol{\nu}} &= 2\,\mathrm{Re}\{(\boldsymbol{C}(\boldsymbol{\tau}) \odot \boldsymbol{D}(\boldsymbol{\nu}))^H \boldsymbol{\Psi}(\boldsymbol{\tau},\boldsymbol{\nu})\} \\
\boldsymbol{F}_{\mathrm{Im}\{\boldsymbol{\gamma}\}\boldsymbol{\tau}} &= 2\,\mathrm{Re}\{-\mathrm{j}\,(\boldsymbol{C}(\boldsymbol{\tau}) \odot \boldsymbol{D}(\boldsymbol{\nu}))^H \boldsymbol{\Upsilon}(\boldsymbol{\tau},\boldsymbol{\nu})\} \\
\boldsymbol{F}_{\mathrm{Im}\{\boldsymbol{\gamma}\}\boldsymbol{\nu}} &= 2\,\mathrm{Re}\{-\mathrm{j}\,(\boldsymbol{C}(\boldsymbol{\tau}) \odot \boldsymbol{D}(\boldsymbol{\nu}))^H \boldsymbol{\Psi}(\boldsymbol{\tau},\boldsymbol{\nu})\} \\
\boldsymbol{F}_{\boldsymbol{\tau}\boldsymbol{\nu}} &= 2\,\mathrm{Re}\{\boldsymbol{\Upsilon}^H(\boldsymbol{\tau},\boldsymbol{\nu})\boldsymbol{\Psi}(\boldsymbol{\tau},\boldsymbol{\nu})\}
\end{aligned}
$$

with

$$
\boldsymbol{\Upsilon}(\boldsymbol{\tau},\boldsymbol{\nu}) = \left[\frac{\partial \boldsymbol{c}_1(\tau_1)}{\partial \tau_1} \odot \boldsymbol{d}(\nu_1), \ldots, \frac{\partial \boldsymbol{c}_K(\tau_K)}{\partial \tau_K} \odot \boldsymbol{d}(\nu_K)\right] \mathrm{diag}\{\boldsymbol{\gamma}\}
$$

$$
\boldsymbol{\Psi}(\boldsymbol{\tau},\boldsymbol{\nu}) = \left[\boldsymbol{c}_1(\tau_1) \odot \frac{\partial \boldsymbol{d}(\nu_1)}{\partial \nu_1}, \ldots, \boldsymbol{c}_K(\tau_K) \odot \frac{\partial \boldsymbol{d}(\nu_K)}{\partial \nu_K}\right] \mathrm{diag}\{\boldsymbol{\gamma}\}
$$

containing the partial derivatives

$$
\begin{aligned}
\frac{\partial \boldsymbol{c}_k(\tau_k)}{\partial \tau_k} &= \left[-\frac{\mathrm{d}}{\mathrm{d}t}c_k(t)\Big|_{t=-\tau_k}, \ldots, -\frac{\mathrm{d}}{\mathrm{d}t}c_k(t)\Big|_{t=(N-1)T_s-\tau_k}\right]^T \\
\frac{\partial \boldsymbol{d}(\nu_k)}{\partial \nu_k} &= \left[0, \ldots, \mathrm{j}2\pi(N-1)T_s e^{\mathrm{j}2\pi\nu_k(N-1)T_s}\right]^T. \qquad (22)
\end{aligned}
$$

VII. Algorithm

Due to the dimension of the argument and the nonlinearity of the estimator (16) in $\boldsymbol{\tau}$, $\boldsymbol{\nu}$, the required maximization for the joint estimator is computationally complex. Therefore, an iterative algorithm based on Space-Alternating Generalized Expectation-Maximization (SAGE) [6] is used to calculate the estimator. Instead of directly maximizing $\Phi(\boldsymbol{\tau},\boldsymbol{\nu};\boldsymbol{y})$ with respect to $\boldsymbol{\tau},\boldsymbol{\nu}$, the algorithm performs the optimization based on objective functions with low-dimensional arguments

$$
\phi_k(\tau,\nu;\hat{\boldsymbol{y}}_k) = \frac{\left|\hat{\boldsymbol{y}}_k^H(\boldsymbol{c}_k(\tau) \odot \boldsymbol{d}(\nu))\right|}{\|\boldsymbol{c}_k(\tau)\|}. \qquad (23)
$$

The parameters τ, ν are associated with the time-delay and Doppler-shift of the k-th satellite while $\hat{\boldsymbol{y}}_k$ is an auxiliary receive signal without the estimated interference of the other $K-1$ satellites

$$
\hat{\boldsymbol{y}}_k = \boldsymbol{y} - \sum_{\substack{\kappa=1 \\ \kappa\neq k}}^{K} \boldsymbol{s}_\kappa(\hat{\boldsymbol{\theta}}_\kappa). \qquad (24)
$$

Algorithm 1 can be used to obtain a high resolution solution to the estimation problem (16). The procedure guarantees convergence to a local optimum of the ML function and can be initiated appropriately with $\hat{\boldsymbol{\theta}}_{\mathrm{IN}}$, calculated by Algorithm 2. While the time-delay and Doppler-shifts are estimated by determining the maximum of a correlation function, the interference of already estimated signal components is successively canceled.

Algorithm 1 Iterative Multi-Satellite TDE with SAGE

$\hat{\boldsymbol{\theta}} := \hat{\boldsymbol{\theta}}_{\mathrm{IN}}$
for $l = 1$ **to** L **do**
  for $k = 1$ **to** K **do**
    $\hat{\boldsymbol{y}}_k := \boldsymbol{y} - \sum_{\substack{\kappa=1 \\ \kappa\neq k}}^{K} \boldsymbol{s}_\kappa(\hat{\boldsymbol{\theta}}_\kappa)$
    $\hat{\tau}_k := \arg\max_{\tau} \phi_k(\tau, \hat{\nu}_k; \hat{\boldsymbol{y}}_k)$
    $\hat{\nu}_k := \arg\max_{\nu} \phi_k(\hat{\tau}_k, \nu; \hat{\boldsymbol{y}}_k)$
    $\hat{\gamma}_k := \frac{(\boldsymbol{c}_k(\hat{\tau}_k) \odot \boldsymbol{d}(\hat{\nu}_k))^H \hat{\boldsymbol{y}}_k}{\|\boldsymbol{c}_k(\hat{\tau}_k)\|^2}$
  end for
end for
$\hat{\boldsymbol{\theta}}_{\mathrm{ML}} := \hat{\boldsymbol{\theta}}$

Algorithm 2 Initialization Multi-Satellite TDE

$\hat{\boldsymbol{\theta}} := \boldsymbol{0}$
for $k = 1$ **to** K **do**
  $\hat{\boldsymbol{y}}_k := \boldsymbol{y} - \sum_{\substack{\kappa=1 \\ \kappa\neq k}}^{K} \boldsymbol{s}_\kappa(\hat{\boldsymbol{\theta}}_\kappa)$
  $(\hat{\tau}_k, \hat{\nu}_k) := \arg\max_{(\tau,\nu)} \phi_k(\tau, \nu; \hat{\boldsymbol{y}}_k)$
  $\hat{\gamma}_k := \frac{(\boldsymbol{c}_k(\hat{\tau}_k) \odot \boldsymbol{d}(\hat{\nu}_k))^H \hat{\boldsymbol{y}}_k}{\|\boldsymbol{c}_k(\hat{\tau}_k)\|^2}$
end for
$\hat{\boldsymbol{\theta}}_{\mathrm{IN}} := \hat{\boldsymbol{\theta}}$

VIII. GNSS Signals

For simulations GNSS signals of GPS and Galileo are used. For GPS L1 C/A the satellite signals are generated with

$$
c_k(t) = \sum_{q=-\infty}^{+\infty} d_{k,q}\; g(t - qT_c), \quad k = 1, \ldots, K. \qquad (25)
$$

$d_{k,q} \in \{-1, 1\}$ is the q-th element of the k-th satellites unique binary PR sequence [19] of length 1023 with chip-duration $T_c = 977.52$ ns. Further, $g(t)$ is the band-limited version of

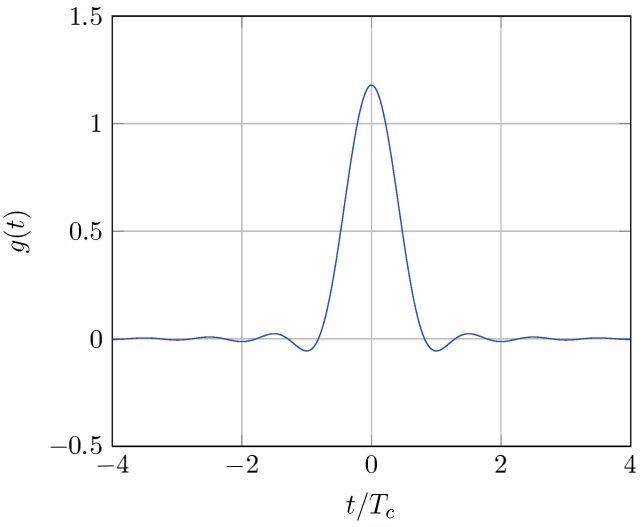

Fig. 2. Bandlimited rectangular chip pulse

the rectangular chip pulse shape for a receiver front-end with bandwidth $B = 1.023$ MHz, which is shown in Fig. 2 and

given analytically by [20]

$$g(t) = \frac{1}{\pi}\left[\mathrm{Si}\left(2\pi B\left(t + \frac{T_c}{2}\right)\right) - \mathrm{Si}\left(2\pi B\left(t - \frac{T_c}{2}\right)\right)\right]$$

with the sine integral

$$\mathrm{Si}(t) = \int_0^t \frac{\sin(\tilde{t})}{\tilde{t}}\,\mathrm{d}\,\tilde{t}.$$

For GPS L1C and Galileo E1 OS Multiplexed BOC (MBOC) signals $c_k(t)$ are generated like for GPS L1 C/A by following the specifications [21] [22].

IX. Simulation Results

In order to evaluate the performance of both approaches, the estimation is performed for different scenarios. As an appropriate figure of merit we employ the mean squared error (MSE), which is given by the diagonal entries of the matrix

$$\mathrm{E}\left[\left(\hat{\boldsymbol{\theta}} - \boldsymbol{\theta}\right)\left(\hat{\boldsymbol{\theta}} - \boldsymbol{\theta}\right)^T\right] \in \mathbb{R}^{4K\times 4K}. \tag{26}$$

We basically focus on the time-delay estimation error of one particular reference satellite, for instance $k = 1$

$$\mathrm{MSE}(\hat{\tau}_1) \triangleq \mathrm{E}\left[(\hat{\tau}_1 - \tau_1)^2\right], \tag{27}$$

which corresponds to the first diagonal entry of the matrix (26). To characterize the performance on average, the parameters time-delay, Doppler-shift and carrier-phase are simulated as i.i.d. uniformly distributed random variables with $\tau_k \in [0, T_k]$, $\nu_k \in [-6\mathrm{kHz}, 6\mathrm{kHz}]$ and $\arg(\gamma_k) \in [0, 2\pi]$ for $k = 1, \ldots, K$ for each Monte Carlo run. Here T_k denotes the period of the k-th satellite signal. If the considered satellites are of the same system T_k is equal for all. Before using the high-resolution algorithm we assume that a conventional signal acquisition algorithm [23] reduces the time and Doppler-shift uncertainty. In each scenario the amplitude $|\gamma_k|$ is specified by the carrier-to-noise density C_k/N_0 of the k-th satellite based on the relation

$$10\log_{10}\left(|\gamma_k|^2\right) = C_k/N_0 - 10\log_{10}(2B). \tag{28}$$

A. Intrasystem Interference

First the focus lies on intrasystem interference in GPS L1 C/A. Therefore, four different scenarios are considered:

1) Increasing Power of the Reference Satellite: In order to identify the gain of joint parameter estimation, the estimation performance (27) is measured while the interfering satellites $k = 2, \ldots, K$ are kept fixed at $C_k/N_0 = 51.5$ dB-Hz and C_1/N_0 of the reference satellite is increased from 48.5 to 51.5 dB-Hz. Therefore, the satellite of interest increases its power level while the remaining satellites stay fixed. The received signal is observed for $T_k = 1$ ms, resulting in $N = 2046$ samples. In Fig. 3, the performance of both estimators in the presence of $K = 6$ satellites is shown and compared to the CRLB. The benefit of joint estimation for six satellites is here equivalent to approximately 1 dB received power. Moreover, joint estimation with SAGE can be considered efficient as the CRLB is attained.

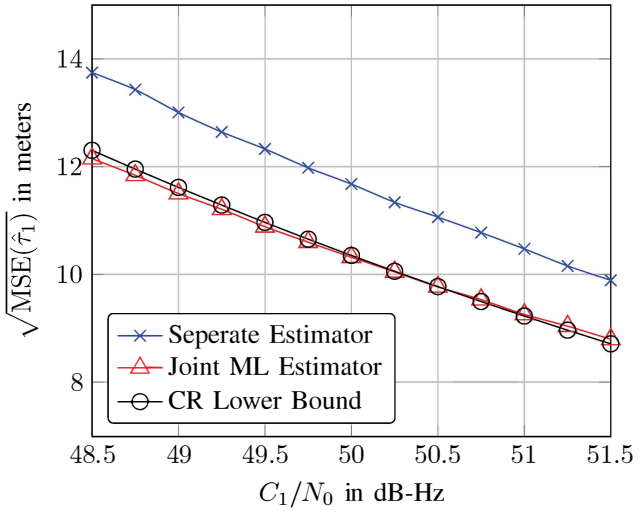

Fig. 3. Estimation performance vs. C_1/N_0

2) Increasing Power of Interfering Satellites: The estimation performance (27) for $K = 6$ is now observed as a function of the power level of interfering satellites. Contrary to the first scenario, the power level of satellite 1, the reference satellite, is kept fixed at 51.5 dB-Hz, while the power of the remaining satellites is increased. Although this situation might lead to a better estimation of $\tau_2, \ldots, \tau_K$, the accuracy of $\hat{\tau}_{1,\mathrm{SEP}}$ degrades (Fig. 4) as the reference satellite suffers from raised interference. The joint estimator, on the other hand, performs robustly in the presence of interferers.

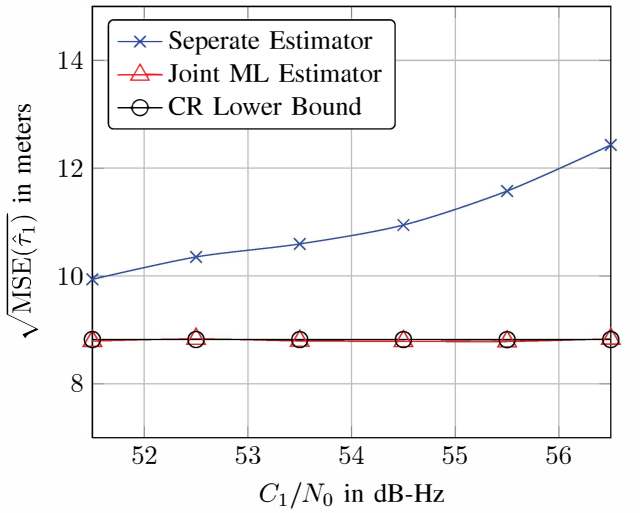

Fig. 4. Estimation performance vs. C_k/N_0

3) Increasing Total Number of Satellites: The effect of intrasystem interference becomes more important as the number of in-view satellites increases (Fig. 5). We choose $C_k/N_0 = 51.5$ dB-Hz for $k = 1, \ldots, K$ and observation duration 1 ms, while the total number of satellites K varies from 1 up to 12. It is observed that the joint estimator achieves the CRLB independently of the number of interfering satellites. This result suggests that the number of practically interfering satellites, regardless if from the same system or not, is irrelevant with

respect to time-delay estimation performance as long as the structure of all incoming signals is known and taken into account at the receiver.

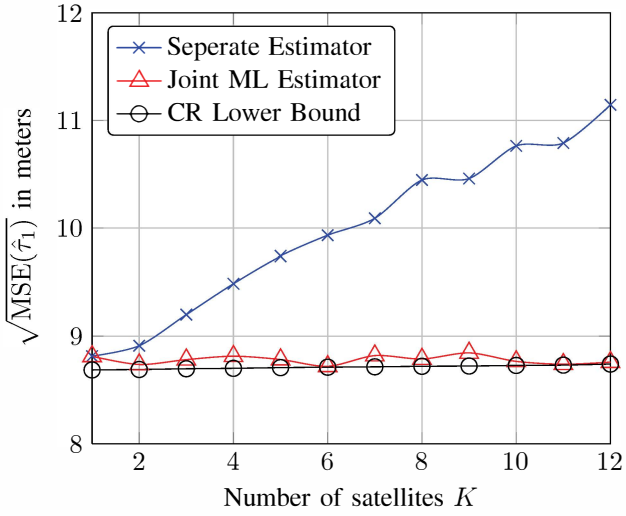

Fig. 5. Increasing number of satellites

4) Increasing Observation Time: The previous simulations were performed for an observation time of 1 ms, i.e., the received signal was observed for a very short duration of one code-period. For this scenario, again all satellites have equal $C_k/N_0 = 51.5$ dB-Hz, but the TDE performance is now calculated for different observation times of 2, 3 and 4 code-period (Fig. 6). While by averaging over a longer observation time the effect of thermal noise becomes less pronounced, the effect of intrasystem interference remains unchanged. The simulation shows that it is not possible to overcome the degradation due to MAI by observing the received signal for a longer time.

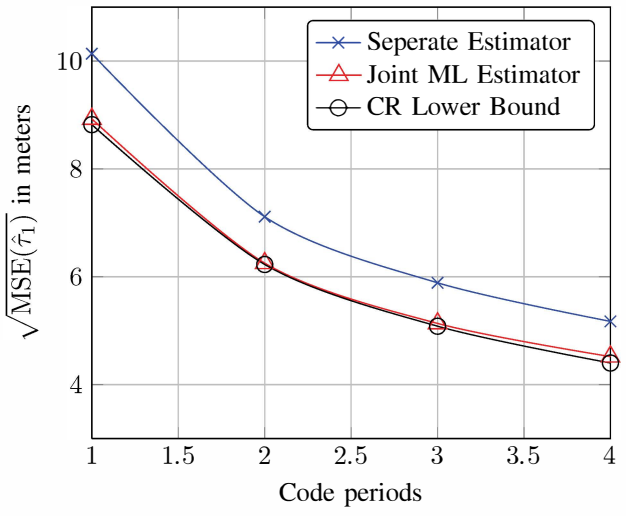

Fig. 6. Increasing observation time

B. Intersystem Interference

The investigation of intersystem interference is of special interest for the new interoperable civilian signals GPS L1C and Galileo E1 OS, as these two signals feature a similar power spectrum. In Fig. 7, the time-delay estimation performance (27) is observed for an intra and intersystem interference scenario of 6 Galileo satellites ($k = 1, \ldots, 6$) transmitting E1 OS pilot and data component with period $T_k = 4$ ms and 6 GPS satellites ($k = 7, \ldots, 12$) transmitting L1C pilot and data component with period $T_k = 10$ ms. Here, we assume a coherent integration time over one Galileo code period of 4 ms while the receiver front-end bandwidth B is set to 2×1.023 MHz. Like in the first scenario, the power level of a Galileo reference satellite is increased while $C_k/N_0 = 51.5$ dB-Hz of all other Galileo and GPS satellites $k = 2, \ldots, 12$ are kept fixed. Consequently, for this scenario intrasystem interference is introduced by Galileo satellites and intersystem interference is caused by GPS satellites. Although, in comparison to the simulations for GPS L1 C/A, the estimation variance of both estimators is reduced due to a larger bandwidth B and observation time, the effect of interference is considerable, resulting in a 1.75 dB gain of the proposed approach over the conventional estimation procedure for this scenario.

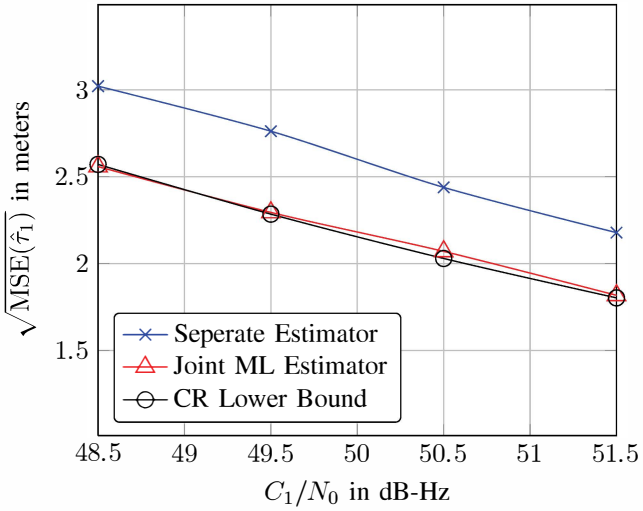

Fig. 7. Estimation performance vs. C_1/N_0

X. Conclusion

In this work, a high resolution joint parameter estimation method for K satellites has been presented and evaluated. Inter- and intrasystem interference which result from the lack of orthogonality between the transmit signals of distinct satellites and systems degrades the estimation accuracy of current GNSS receivers. By taking into account mutual interference at the receiver with the proposed joint estimation procedure, simulations indicate that it is possible to outperform the traditional scheme of estimating each satellite separately which does not take into account the interference. The joint approach performs robustly with respect to the number of interferers and their signal power, whereas the performance of the separate approach degrades significantly. Through an iterative algorithm the complexity of both approaches can be kept similar. In order to fully benefit from the joint approach

the signal structure of all satellites has to be available at the GNSS receiver.

REFERENCES

[1] S. Verdu, Optimum Multiuser Signal Detection, Ph.D. dissertation, University of Illinois, Urbana-Champaign, August 1984.

[2] M.K. Varanasi, B. Aazhang, "Multistage Detection in Asynchronous Code-Division Multiple-Access Communications," *IEEE Transactions on Communications*, vol. 38, no. 4, pp. 509–519, April 1990.

[3] F. Zanier, G. Bacci, M. Luise, "Criteria to Improve Time-Delay Estimation of Spread Spectrum Signals in Satellite Positioning," *IEEE Journal of Selected Topics in Signal Processing*, vol. 3, no. 5, pp. 748–763, October 2009.

[4] F. Antreich and J.A. Nossek, "Optimum chip pulse shape design for timing synchronization," *IEEE International Conference on Acoustics, Speech and Signal Processing (ICASSP), 2011*, pp. 3524–3527, May 2011

[5] M. R. Gupta, Y. Chen, "Theory and Use of the EM Algorithm," *Foundations and Trends in Signal Processing*, vol. 4, no. 3, pp. 223–296, 2010.

[6] J. A. Fessler, A. O. Hero, "Space-Alternating Generalized Expectation-Maximization Algorithm," *IEEE Transactions on Signal Processing*, vol. 42, no. 10, pp. 2664–2677, October 1994.

[7] P. Closas, C. Fernandez-Prades, J. A. Fernandez-Rubio, "Maximum Likelihood Estimation of Position in GNSS," *IEEE Signal Processing Letters*, vol. 14, no. 5, pp. 359–362, May 2007.

[8] L. Jing, C. Xiaowei, C. Qiang, L. Mingquan, "Joint Vector Tracking Loop in a GNSS Receiver," *Proceedings of the 2011 International Technical Meeting of The Institute of Navigation*, San Diego, CA, pp. 1025-1032, January 2011.

[9] K. Giger, C. Günther, "Position Domain Joint Tracking," *5th ESA Workshop on Satellite Navigation Technologies and European Workshop on GNSS Signals and Signal Processing (NAVITEC)*, pp. 1–8, December 2010.

[10] J. J. Spilker, "Global Positioning System: Theory and Applications, Volume I," American Institute of Aeronautics & Astronautics, 1996.

[11] M. Lashley, D. M. Bevley, J. Y. Hung, "A Valid Comparison of Vector and Scalar Tracking Loops," *Position Location and Navigation Symposium (PLANS), IEEE/ION*, pp. 464 – 474, May 2010.

[12] A. L. Swindlehurst, "Time Delay and Spatial Signature Estimation Using Known Asynchronous Signals," *IEEE Transactions on Signal Processing*, vol. 46, no. 2, pp. 449 – 462, February 1998.

[13] G. Seco, A. L. Swindlehurst, and D. Astely, "Exploiting Antenna Arrays for Synchronization," in *Signal Processing Advances in Wireless and Mobile Communications, Volume 2: Trends in Single- and Multi-User Systems*, G. B. Giannakis, P. Stoica, Y. Hua, and L. Tong, Eds. Prentice-Hall, pp. 403 – 430, 2000.

[14] G. Seco-Granados, J. A. Fernandez-Rubio, and C. Fernandez-Prades, "ML Estimator and Hybrid Beamformer for Multipath and Interference Mitigation in GNSS Receivers," *IEEE Transactions on Signal Processing*, vol. 53, no. 3, pp. 1194 – 1208, March 2005.

[15] F. Antreich, J.A. Nossek, G. Seco-Granados, A.L. Swindlehurst, "The Extended Invariance Principle for Signal Parameter Estimation in an Unknown Spatial Field," *IEEE Transactions on Signal Processing*, vol. 59, no. 7, pp. 3213 – 3225, July 2011.

[16] G. Seco-Granados, J.A. Lopez-Salcedo, D. Jimenez-Banos, G. Lopez-Risueno, "Challenges in Indoor Global Navigation Satellite Systems: Unveiling its core features in signal processing," *IEEE Signal Processing Magazine*, vol. 29, no. 2, pp. 108 –131, 2012.

[17] J. V. Perello Gisbert, "Interference Assessment Using up to date Public Information of Operating and under Development RNSS Systems," *Fourth European Workshop GNSS Signals*, 2009.

[18] S. M. Kay, "Fundamentals of Statistical Signal Processing: Estimation Theory," Prentice Hall PTR, 1993.

[19] "NAVSTAR GPS Space Segment/Navigation User Interfaces," IS-GPS-200, Rev. D, ARINC Engineering Services, El Segundo, CA, 2004.

[20] F. Antreich, "Array Processing and Signal Design for Timing Synchronization," Dissertation, Technische Universität München, 2011.

[21] "European GNSS (Galileo) Open Service - Signal In Space Interface Control Document," Issue 1.1, European Union, September 2010.

[22] "NAVSTAR GPS Space Segment/User Segment L1C Interface," IS-GPS-800, Rev. A, Science Applications International Corporation, El Segundo, CA, 2010.

[23] P. Misra, P. Enge, "Global Positioning System: Signals, Measurements, and Performance," Ganga-Jamuna Press, 2001.